Shock Waves (2010) 20:353–366
DOI 10.1007/s00193-010-0269-8

ORIGINAL ARTICLE

Methodology of a combined ground based testing and numerical modelling analysis of supersonic combustion flow paths

Klaus Hannemann · Sebastian Karl · Jan Martinez Schramm · Johan Steelant

Received: 14 January 2010 / Revised: 3 June 2010 / Accepted: 24 June 2010 / Published online: 11 August 2010

Abstract In the framework of the European Commission co-funded LAPCAT (Long-Term Advanced Propulsion Concepts and Technologies) project, the methodology of a combined ground-based testing and numerical modelling analysis of supersonic combustion flow paths was established. The approach is based on free jet testing of complete supersonic combustion ramjet (scramjet) configurations consisting of intake, combustor and nozzle in the High Enthalpy Shock Tunnel Göttingen (HEG) of the German Aerospace Center (DLR) and computational fluid dynamics studies utilising the DLR TAU code. The capability of the established methodology is demonstrated by applying it to the flow path of the generic HyShot II scramjet flight experiment configuration.

Keywords Ground based testing · Computational fluid dynamics · Combustion modelling · Supersonic combustion ramjet · Short duration impulse facility · High enthalpy shock tunnel

Communicated by R.R. Boyce.

The present article is based on the content of a plenary lecture held during the 27th International Symposium on Shock Waves, St. Petersburg, Russia, 19–24 July 2009.

K. Hannemann (✉) · S. Karl · J. Martinez Schramm
German Aerospace Center DLR, Institute of Aerodynamics and Flow Technology, Bunsenstraße 10, 37073 Göttingen, Germany
e-mail: Klaus.Hannemann@dlr.de

J. Steelant
Section of Aerothermodynamics and Propulsion Analysis, European Space Research and Technology Center, 2200 AG Noordwijk, The Netherlands

1 Introduction

In order to reduce the travelling time of long-distance flights, e.g. Brussels to Sydney, to less than four hours, advanced propulsion concepts and technologies need to be developed for flight regimes with Mach numbers ranging from 4 to 8. The supersonic combustion ramjet (scramjet) engine represents a potential component in a combined cycle propulsion system to achieve this goal. The subject of the LAPCAT project of the 6th European Framework Program was the development of key technologies for advanced high-speed airbreathing propulsion systems [1]. Two different hypersonic transport vehicle concepts were considered. The first is an aircraft with a maximum cruise Mach number of $M = 5$, powered by four individual pre-cooled turbofan-ramjet engines and the second is a hypersonic aircraft configuration utilising a propulsion system which is fully integrated into the airframe [1]. The latter aims at flight velocities up to $M = 8$ and is propelled with a combination of air turbo rocket and dual mode ram-/scramjet engines [2] (Fig. 1).

Although significant advances were made in developing scramjet engines, including the University of Queensland's supersonic combustion flight experiment program HyShot with four launches in 2001, 2002 and 2006 (see e.g. [3–5]) and two flights of NASA's X-43 in 2004 (see e.g. [6]), major scientific and technological challenges remain.

Due to the fact that with increasing flight Mach number the difference between engine entrance and thrust nozzle exit velocity decreases relative to the flight velocity, a positive aero-propulsive balance can only be achieved if the aerodynamic drag is minimised and the thrust is maximized. Therefore, the design objective for a scramjet engine is a combustor with the shortest possible length while still allowing efficient mixing and complete combustion.

Fig. 1 LAPCAT $M = 8$ vehicle configuration

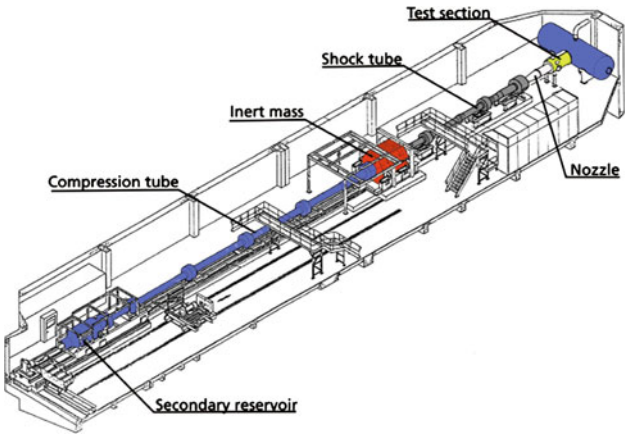

Fig. 2 Schematic of the High Enthalpy Shock Tunnel Göttingen (HEG)

The complexity of the flows in airbreathing propulsion systems of advanced hypersonic transport vehicles requires a strong link of ground-based experiments, computational fluid dynamics and flight testing in order to improve the understanding of flow phenomena such as fuel mixing, ignition delay and unstart.

In the framework of LAPCAT, emphasis was put on the development, verification and validation of free jet ground-based test capabilities and numerical tools to study scramjet flow paths. Further, a methodology was established to efficiently combine experiments and computational fluid dynamics (CFD). To demonstrate the capability of this methodology, the HyShot II flight test configuration was selected. This generic scramjet consisting of intake, combustor and nozzle was designed such that it contains all necessary components of a scramjet but still generates an overall flow field which is as simple as possible with a well defined combustor inflow. Therefore, it was considered to be a configuration well suited for basic investigations and tool validation purposes. Further, the goal of the HyShot flight program performed by The University of Queensland in Australia together with an international consortium was to provide benchmark data on supersonic combustion for a flight Mach number of approximately $M = 8$. While it is the ultimate goal to compare ground-based test data and numerical results with flight data, this step could not be accomplished for the set of data presented here. The reason for this is that the present investigations focused on a flight trajectory point in an altitude of 28 km and the detailed analysis of the HyShot II flight data [4] led to the conclusion that structural integrity of the flight model was compromised below 30 km. Therefore, no comparison of the obtained experimental and numerical data with flight data was performed.

The experimental investigations of the HyShot II scramjet flight test configuration utilising a 1:1 scale wind tunnel model were carried out in the High Enthalpy Shock Tunnel Göttingen (HEG) [7–9]. In general, shock tunnel facilities deliver test times in the order of milliseconds. However, in comparison to blow down free jet scramjet test facilities such as the Ramjet Engine Test Facility (RJTF) of the Japan Aerospace Exploration Agency (JAXA) [10] or the Aerodynamic and Propulsion Test Unit (APTU) at the Arnold Engineering Development Center (AEDC) [11] with test times in the order of minutes, the simulated flight Mach number range of shock tunnels is not limited to $M = 8$. This is of particular interest when exploring the potential of scramjet engines not only for hypersonic transport but also for future space launchers. For $M = 8$ flight condition the operating range of both types of facilities overlap. Therefore, this condition is of particular interest because it is suited to perform facility crosschecks.

For the numerical investigations, the DLR CFD tool TAU [12,13], which was extended in the framework of LAPCAT to allow the computation of turbulent supersonic combustion of a gaseous hydrogen/air mixture was utilised.

The main objective of the present article is focused on the demonstration of the established methodology to study scramjet flow paths. The experiments and CFD studies performed during the LAPCAT project included detailed parameter studies and variations of the numerical model. Only selected results of the determination of HEG test section free-stream conditions and of fuel-off and fuel-on HyShot II flow path studies are presented here.

2 Experimental and numerical tools

2.1 High Enthalpy Shock Tunnel Göttingen

The HEG is a free-piston-driven shock tunnel [7,8] which was designed and built over the period 1989–1991 and was commissioned for use in 1991, at that time being the largest free-piston-driven shock tunnel worldwide (see Figs. 2, 3).

The facility is operated in reflected mode. It is designed to provide a pulse of gas to a nozzle at stagnation pressures of

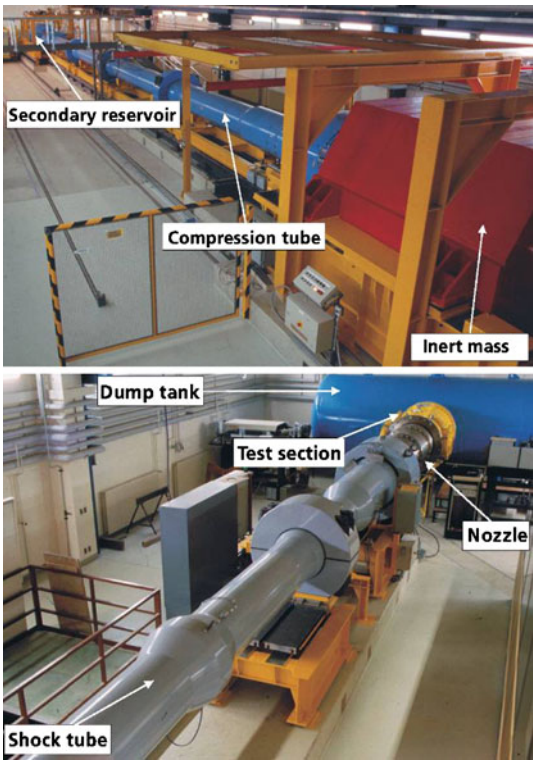

Fig. 3 Photographic views of HEG

up to 200 MPa, and stagnation enthalpies of up to 24 MJ/kg. Since its commissioning in the early 1990s, HEG has been utilised in numerous space and hypersonic flight programs. The research activities which were always strongly linked with CFD investigations range from the calibration process of the facility and the study of basic aerodynamic configurations, which are well suited to investigate fundamental aspects of high-enthalpy flows, to the investigation of complex re-entry configurations.

An overview of the facility details is given by the schematic in Fig. 2 and the pictures in Fig. 3. The overall length of the facility is 60 m and it weighs 280 t. Due to the resulting forces of the piston motion the whole facility moves on a rail and bearing system. Approximately a third of its weight is contributed by an inert mass which is used to reduce the tunnel recoil motion. The HEG facility consists of a secondary reservoir, a compression tube, separated from an adjoining shock tube via the primary diaphragm and a subsequent nozzle and test section. The high-pressure air in the secondary reservoir drives the piston down the compression tube which is closed by a hydraulic oil system (quick disk connect) at the main diaphragm station. The shock tube is connected to the nozzle of the tunnel at the downstream closure, which is also driven by oil hydraulics to close and seal the tunnel. Additional information about HEG is given in [7,8].

Recent extensions to the HEG operating range now allow ground-based testing of complete scramjet engines. The

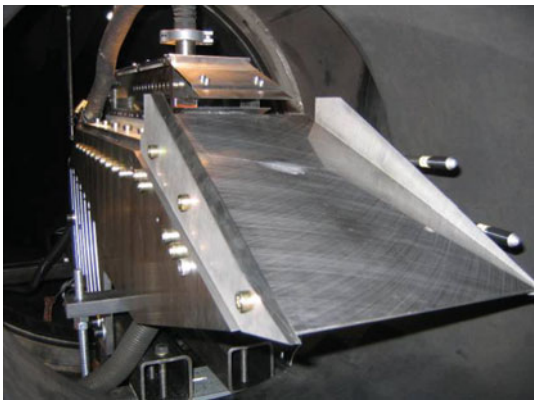

Fig. 4 HyShot wind tunnel model installed in the HEG test section

extensions included the design and construction of a contoured nozzle which provides nominal parallel Mach 7.4 flow with a test core of 400- mm-diameter, the construction of a new 850-kg piston as well as the installation of a fuel system for the delivery of hydrogen fuel to the wind tunnel model. The fuel system consists of a 12- mm-diameter and 38.4 m long Ludwieg tube, and a fast-acting solenoid valve. The maximum filling pressure of the Ludwieg tube is 15 MPa, and it can deliver a pulse of fuel with constant pressure for up to 50 ms. New test conditions at total enthalpies of about 3 MJ/kg were also designed and calibrated.

2.2 HyShot II wind tunnel model

The HyShot II wind tunnel model installed in the HEG test section is shown in Fig. 4. Apart from a wider intake, the geometry of this model is a 1:1 scale representation of the fuelled flow path of the HyShot II scramjet flight test configuration, except for the width of the intake ramp, which was extended from 100 to 196 mm. The reason for this is to avoid detrimental effects on the flow visualization of the combustor flow by the presence of external shocks close to the outer surface of the glass windows.

A cut along the symmetry plane of the HyShot II model configuration assembly is shown in Fig. 5. The cross-sectional shape of the intake and the internal flow path of the wind tunnel model are defined by five parts: the intake ramp, the upper and lower combustion chamber walls and the upper and lower exhaust walls. The intake is a simple 18° wedge. Between the intake and the combustion chamber, a boundary bleed channel is used such that the boundary layer and entropy layer of the intake ramp do not enter the combustor. Further, the bleed allows the shock generated by the leading edge of the cowl to pass outside the combustion chamber. The combustion chamber is parallel and the cross-sectional dimensions are 9.8 $\times$ 75 mm. The length of the constant area combustor is 300.0 mm. Fuel is injected into the

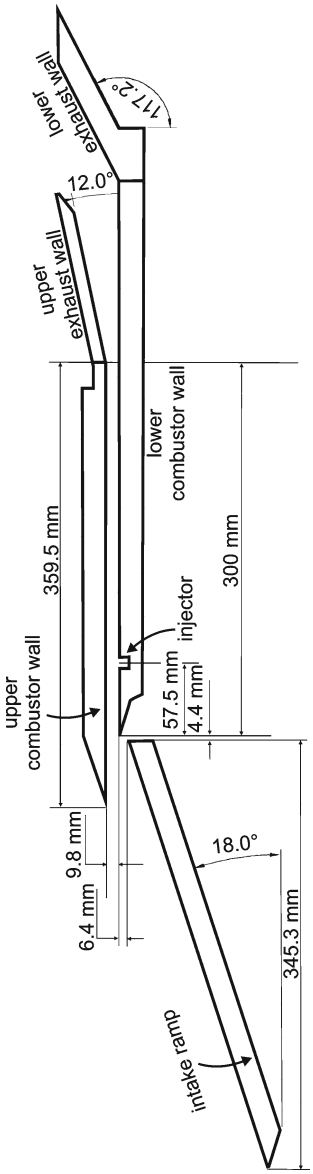

Fig. 5 HyShot II model configuration assembly

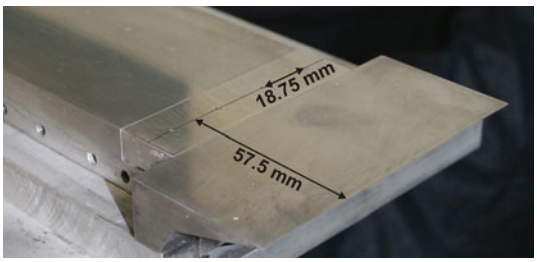

Fig. 6 HyShot II injector block installed in the lower combustion chamber wall

combustion chamber by a series of four holes, with radius of 1 mm, equally spaced along one line in cross flow direction in the lower combustor wall, 57.5 mm downstream of its leading edge (see Fig. 6). The radius of the intake leading edge is 1 mm and the leading edge radius of the upper or lower combustor wall amounts to 0.2 mm.

Pressures on the model were measured using KULITE pressure transducers. A range of pressure transducers is available for use in HEG. Their maximum pressure range varies from 35 to 700 kPa. Typically, KULITE XCS-093 transducers with a diameter of 2.3622 mm are used. The transducer sensitivity is sensor-specific and the calibration factor of each sensor is determined including the whole measurement chain when installed in HEG. The response time of the transducers is about 7 μs. Surface pressure measurements in short-duration facilities have to be based on different approaches than the pressure measurements in continuously running facilities. Therefore, the fast-response pressure transducers are placed close to the model surface in HEG in order to reduce the response time of the integrated system consisting of pressure gauge and gauge mounting.

Wall heat transfer was determined from the measured surface temperature histories. MedTherm coaxial thermocouples with a nominal response time of 1 μs and a sensitivity of 58.8 μV/K were utilized. The thermocouples are manufactured from chromel and constantan and they are mounted flush to the model surface. The model number is TCS-061-E-XX-24-10866 where XX refers to the thermocouple length (2.54–22.86 mm). The thermocouples are NIST type E and have a diameter of 1.549 mm. Type E thermocouples have the highest milli-volt per degree of temperature change output of all base metal thermocouples.

On the intake ramp, five pressure gauges and four thermocouples were integrated along the symmetry line. The upper combustion chamber wall was instrumented with 23 pressure gauges and 11 thermocouples. The pressure transducers were positioned along the symmetry line and the thermocouples along a line 9 mm off the symmetry line. In the lower combustion chamber wall, 31 pressure transducers and 15 thermocouples were integrated. The pressure gauges were positioned along the symmetry line and the thermocouples downstream of a hydrogen injector along a line 10 mm off the symmetry line.

The upper and lower exhaust surfaces were instrumented with five and six pressure transducers, respectively. The origin of the coordinate system used to plot the measured and computed combustion chamber wall pressure and wall heat flux data in the subsequent sections is the leading edge of the lower combustor wall.

2.3 DLR TAU code

The numerical investigations presented here were performed with the hybrid structured/unstructured DLR Euler/Navier–Stokes solver TAU [12,13]. This code was applied and

validated for a wide range of steady and unsteady sub-, trans- and hypersonic flow cases. A nominally second order finite-volume space discretization is applied to solve the Euler and Navier–Stokes equations in the integral form. For the modelling of turbulence, different eddy-viscosity and Reynolds-stress models as well as detached eddy simulation (DES) and large eddy simulation (LES) are used.

The present investigations were performed using the Reynolds averaged Navier–Stokes equations (RANS) and the one-equation Spalart–Allmaras [14] and the two-equation Wilcox k-ω [15] turbulence models. The models were used in low Reynolds number formulation, i.e. no wall functions were applied. The AUSMDV [16] flux vector splitting scheme is applied together with MUSCL gradient reconstruction to achieve second-order spatial accuracy.

The TAU combustion model is based on the modelling of chemical and thermal non-equilibrium flows in high-enthalpy aerothermodynamic environments [13]. The flow is considered to be a reacting mixture of thermally perfect gases. A transport equation is solved for each individual species. The chemical source term in this set of transport equations is computed from the law of mass action by summation over all participating reactions. The forward reaction rate is computed from the modified Arrhenius law and the backward rate is obtained from the equilibrium constant which is computed directly from the partition functions of the participating species. The modified Jachimowski reaction mechanism for hydrogen–air mixtures (see e.g. Gerlinger [17]) was used for the present investigations. This mechanism includes hydrogen peroxide (H_2O_2) and the perhydroxyl radical (HO_2) and is valid over a wide range of pressures, densities and equivalence ratios. The thermodynamic properties (energy, entropy, specific heat) are calculated from the partition functions of each individual species in the reacting gas mixture. The advantage of this approach is its high flexibility. Extensions such as multi-temperature models to handle thermal non-equilibrium effects can easily be implemented. Knowing the mixture composition and the thermodynamic state of the individual species, the properties of the reacting gas mixture are computed using suitable mixture rules such as proposed by Wilke [18] for the viscosity and by Herning and Zipperer [19] for the heat conductivity. For fully catalytic walls, Dirichlet boundary conditions are used for the species mass fractions resulting from the local equilibrium composition. Non-catalytic walls are modelled using von Neumann boundary conditions imposing vanishing wall-normal gradients of the species mass fractions. The species diffusion fluxes are modelled using Fick's law and an averaged diffusion coefficient for all species. This approximate diffusion coefficient is computed using the viscosity and a constant Schmidt number of $Sc = 0.7$. For turbulent flows the viscosity is taken to be the sum of the laminar and the turbulent contributions. The turbulent viscosity is derived from the applied turbulence model (e.g. computed from turbulent kinetic energy and length scale for the application of the k-ω model or directly obtained from the Spalart–Allmaras model). Thermal non-equilibrium flows are computed by solving an additional transport equation for the vibrational energy of each molecule in non-equilibrium. The relaxation of vibrational energy is modelled according to the Landau–Teller [20] approach, and the vibrational relaxation times are obtained from the correlation of Millikan and White [21]. An assumed probability-density-function (PDF) model as described by Gerlinger [17] was additionally implemented in order to model the interaction of turbulence and chemistry. The averaged turbulent chemical source terms are computed by integrating the laminar expression over all realizable temperatures and species concentrations which are weighted by the probability of their occurrence. These probabilities are given by presumed shape PDFs (Gaussian distribution for the temperature and multi-variate beta distributions for the species concentrations). Statistical independence of temperature and species concentration fluctuations is assumed. Two additional transport equations for the variance of temperature and the sum of the variances of species concentrations are solved to completely describe the PDF at each point of the flow field.

Advantages of the described combustion model are that it can be applied for premixed, non-premixed or partially premixed flames and that no limitations concerning the range of Damköhler number exists. Further, the implementation in a chemical non-equilibrium flow solver is straightforward and the approach is highly robust and numerically efficient. The successful application to supersonic combustion problems was already demonstrated [17,22].

3 Experimental and numerical scramjet flow path investigations

The experimental and numerical treatment of scramjet flow paths generated in ground-based test facilities closely depends on the utilisation of a suitable and correct set of free stream data. In addition to the free-stream Mach number and the unit Reynolds number, the knowledge of the absolute values of the free-stream pressure and temperature are of particular importance since they determine via the intake flow the combustor inflow condition which in turn have a strong influence on the combustion process. Therefore, the present approach is split up in three main steps, namely

- Determination of the HEG free stream flow;
- Analysis of the intake flow;
- Analysis of the combustor and nozzle flow.

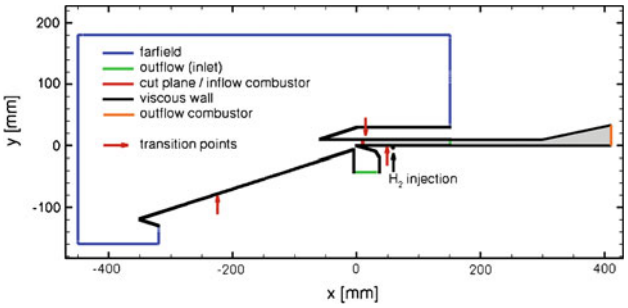

Fig. 7 Computational domains and boundary conditions used for the intake and combustor/nozzle investigations

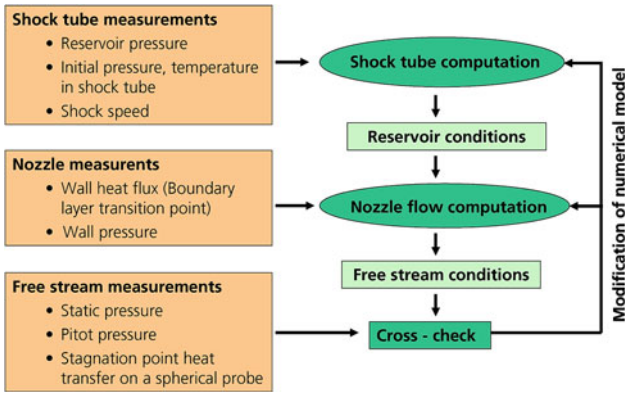

Fig. 8 Combined experimental and numerical iterative procedure to determine HEG free-stream conditions

In principle, an integrated computation of the facility nozzle flow and the complete scramjet flow path could be performed. However, in order to sufficiently resolve all important flow features, this approach would be very time consuming and would not allow that systematic parameter and numerical model variations are performed. The aforementioned stepwise approach ensures that specific characteristics of the considered flow fields such as symmetries can be used to perform economic computations.

The computational domains and the applied boundary conditions used to study the intake and the combustor/nozzle flow fields of the HyShot II configuration are sketched in Fig. 7 in a plane cutting through an injector. During the short test time in HEG, no significant heating of the model walls occurs. Therefore, the walls were assumed to be isothermal at a temperature of 300 K and non-catalytic. The HEG free stream used for the present studies is related to a flight trajectory point of HyShot II in an altitude of 28 km. From the flight data [26], an angle of attack of $\alpha = 3.6°$ was derived and used for the present studies.

3.1 Determination of the HEG free stream flow

The HEG operating condition XIII [9] was used for the present investigations. It was designed to generate a free stream flow which simulates a HyShot II flight point in an altitude of 28 km. The total available test time is approximately 4 milliseconds. For a test using this condition, a pressure of 1.9 MPa in the air buffer is utilised to accelerate the 850-kg piston down the 33-m-long compression tube. During this compression and heating of the driver gas, the piston reaches a maximum velocity of about 67 m/s. When the burst pressure of the 5- mm-thick stainless steel main diaphragm of 24 MPa is reached, the driver gas, consisting of a helium/argon mixture, is heated up quasi-adiabatically to 1,600 K. After diaphragm rupture a strong shock wave is generated. It propagates down the 17-m-long shock tube with a velocity of approximately 1.8 km/s and reflects from the end wall, heating up the test gas to the required reservoir conditions. Subsequently, the test gas expands through the convergent–divergent contoured hypersonic nozzle with an exit diameter of 0.6 m.

The free stream calibration process for high-enthalpy ground-based test facilities is much more complex than for cold hypersonic facilities. One reason for this is that the behaviour of the test gas deviates from that of a calorically perfect gas. With increasing total enthalpy, the excitation of internal degrees of freedom such as the vibrational excitation of molecules and subsequently chemical reactions must be considered. Additional difficulties arise from the fact that some parts of the HEG facility, such as the nozzle reservoir, are not accessible with modern optical measurement techniques due to limitations caused by their structural design. These result from temperatures of up to 10,000 K and pressures of up to 2,000 bar which are reached at the highest total enthalpy and total pressure conditions. Therefore, the evaluation of the free-stream conditions in the test section of the HEG free-piston-driven shock tunnel is performed by numerical analysis using a suitable set of measured input and reference parameters. The general iterative procedure established to determine HEG free-stream conditions is outlined in Fig. 8.

First, the nozzle reservoir temperature is computed with a one-dimensional simulation of the shock tube using ESTC [7,23]. The relevant input parameters are the measured values of the initial shock tube filling pressure and temperature, the shock speed and the nozzle reservoir pressure. Based on the nozzle reservoir conditions (see Table 1), the free stream is subsequently determined by numerical computation of the nozzle flow utilising the TAU code. The grid consisting of about 20,000 points and Mach number contours, resulting from a computation using the assumption that a thermal non-equilibrium nozzle expansion is established, are shown in Fig. 9.

A reservoir-pressure inflow boundary condition is used at the subsonic inflow of the nozzle. The thermodynamic conditions at the inflow are computed using isentropic expansion

Table 1 Nominal reservoir and averaged free-stream conditions for HEG operating condition XIII

	Condition XIII
Nozzle reservoir pressure, p_0 (MPa)	17.41
Nozzle reservoir temperature, T_0 (K)	2,735
Stagnation enthalpy, h_0 (MJ/kg)	3.30
p_∞ [Pa]	1,988
p_{t2} [kPa]	142
q_{t2}[MW/m^2]	4.38
T_∞ [K]	266
ρ_∞[kg/m^3]	0.0259
u_∞ [m/s]	2,414
M_∞ [–]	7.37
Re_m [1/m]	3.71×10^6

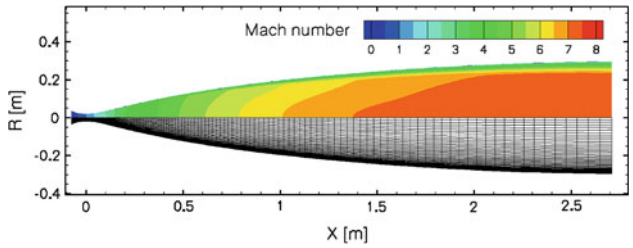

Fig. 9 CFD grid and Mach number contours for the HEG nozzle flow (operating condition XIII)

from prescribed nozzle stagnation conditions using the inflow velocity vector which is part of the CFD solution. The chemical non-equilibrium 5 species and 17 reactions rate set for air proposed by Gupta [24] was applied. Previous studies showed good performance of this model for chemical relaxation in high-enthalpy wind tunnel nozzles [25]. The considered species are molecular and atomic nitrogen and oxygen (N_2, O_2, N, O) and nitric oxide (NO). It should be noted that for the present operating condition, the influence of chemical reactions is considered to be small due to the low reservoir temperature. However, the temperatures are sufficiently high that molecular species are vibrationally excited. Due to the fact that the thermal relaxation behaviour in the nozzle expansion is not known a priori, assumptions of both thermal equilibrium and thermal non-equilibrium were investigated separately in the computations. This sensitivity analysis was performed with a simplified thermal relaxation model for the non-equilibrium case, accounting for vibrational–translational energy transfer only (see also Sect. 2.4). Further, only the aforementioned species are considered and additional ones, which might be present in the flow at low concentrations, were not taken into account; however, their influence on the vibrational relaxation process may be significant. Also, there is some uncertainty in the vibrational relaxation times in the applied non-equilibrium model.

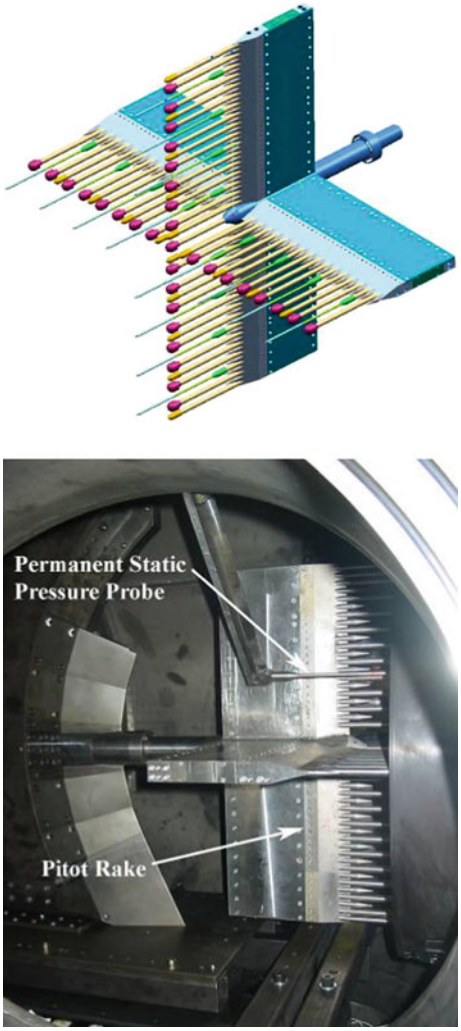

Fig. 10 Calibration rake equipped with Pitot pressure, stagnation point heat transfer and static pressure gauges. Design drawing (*upper*) and rake installed in the HEG test section (*lower*)

The accuracy of this CFD-based approach for the determination of the free-stream conditions was assessed by comparison with available experimental calibration data at the nozzle exit plane. The data were obtained with the calibration rake shown in Fig. 10. Pitot pressure and stagnation point heat flux measurements on spherical probes and static pressure measurements were performed. The comparison between numerical and experimental calibration data also included the computation of the flow past the probes used in HEG [27].

In Fig. 11, the comparison of measured and computed normalised Pitot pressure, static pressure and stagnation point heat transfer profiles at the nozzle exit plane are shown. The data are normalised using the nozzle reservoir pressure and a reference heat flux value derived from the stagnation point heat flux measurements on the spherical calibration probes. The diameter of these probes is 20 mm and the reference heat

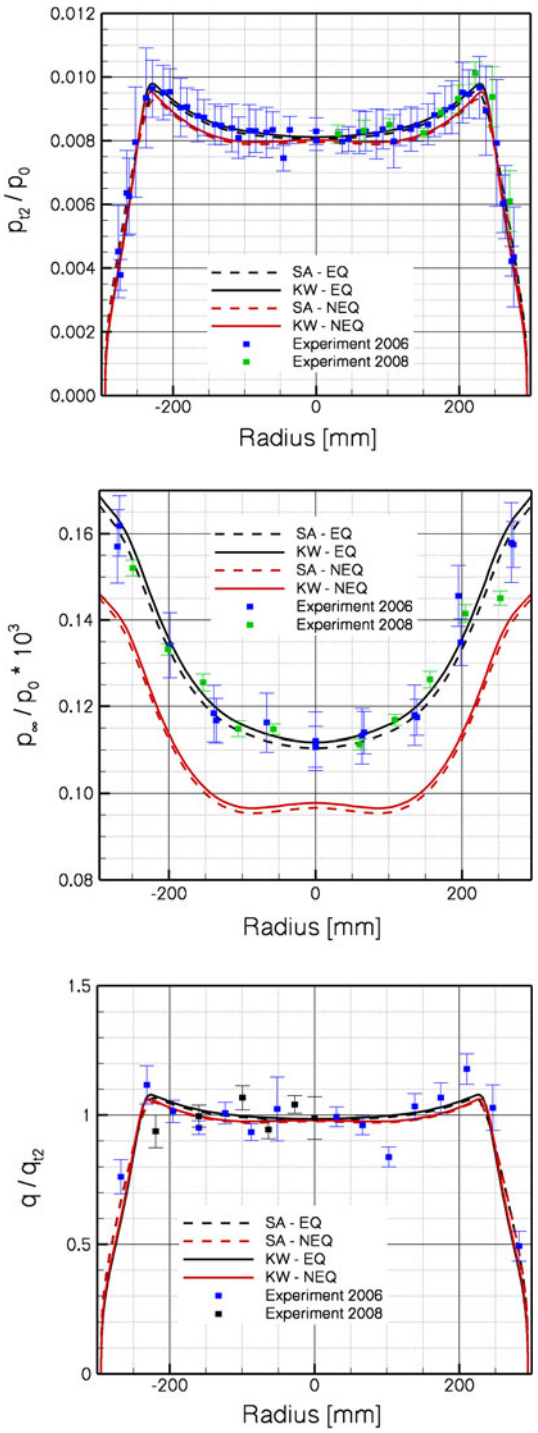

Fig. 11 Comparison of measured and computed normalised Pitot pressure (*upper*), static pressure (*middle*) and stagnation point heat flux distributions (*lower*) at the nozzle exit plane. *NEQ* thermal non-equilibrium, *EQ* thermal equilibrium, *SA* Spalart–Allmaras turbulence model, *KW* Wilcox k-ω turbulence model

flux value, q_{t2}, corresponding to the nominal, averaged free-stream conditions of HEG operating condition XIII is provided in Table 1. Regarding the Pitot pressure, the computed data resulting from computations assuming either a thermal equilibrium or a thermal non-equilibrium nozzle expansion lie within the experimental scatter bars. For the present operating condition, the wall boundary layer is assumed to be fully turbulent and the difference due to the application of different turbulence models is negligible. The excellent reproduction of the measured Pitot pressure profile shape confirms the assumption regarding the state of the boundary layer. The best agreement between computed and average measured Pitot pressure profiles is obtained with the thermal equilibrium assumption.

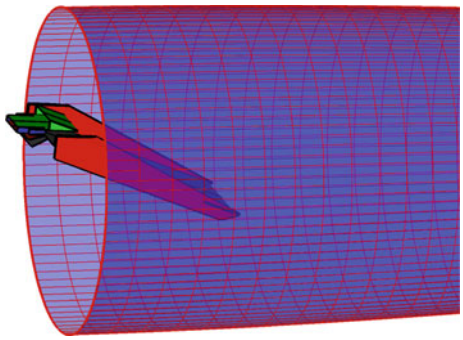

Fig. 12 Position of the HyShot II intake relative to the exit section of the HEG nozzle

The computed static pressure profiles reveal pronounced deviations resulting from the application of different thermal relaxation models. Excellent agreement of the numerical and experimental results was achieved using the thermal equilibrium assumption. The discrepancy between the measured and the non-equilibrium computed values may be due to the limitations of the applied vibrational relaxation model mentioned earlier. These results highlight, however, the importance of the static pressure measurements since they help to select the most suitable numerical model to determine the free stream pressure and consequently the free-stream temperature.

The lower plot of Fig. 11 shows the comparison of the numerical and experimental normalised stagnation point heat flux profiles. Similar to the Pitot pressure, the computed values of this quantity reveal only slight variations when the assumption of a thermal equilibrium or thermal non-equilibrium nozzle expansion is used. The obtained differences lie within the experimental scatter bars.

The nominal nozzle reservoir conditions and averaged free-stream conditions of HEG operating condition XIII are summarized in Table 1.

3.2 Analysis of the intake flow

The intake flow was first investigated by a three-dimensional flow field computation. The inflow conditions were determined by interpolation from the nozzle flow computations discussed in Sect. 3.1. The position of the intake relative to the HEG nozzle exit section is shown in Fig. 12.

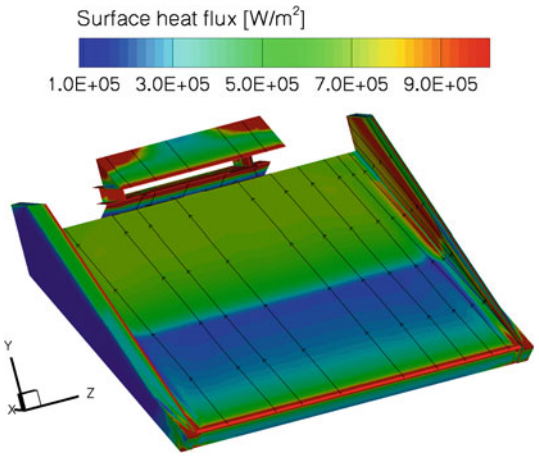

Fig. 13 Skin friction lines and surface heat flux contours on the HyShot II intake ramp

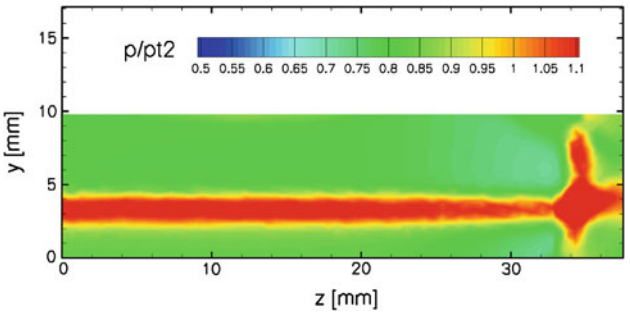

Fig. 14 Normalised pressure distribution in the combustor inflow plane resulting from a three-dimensional intake flow computation

The grid contained 850,000 points. Computed skin friction lines and the surface heat flux distribution on the intake are plotted in Fig. 13. The laminar to turbulent boundary layer transition occurring on the intake ramp was modeled with a criterion taken from [28]. It is based on $[Re_\theta/M_e]_{\text{crit}} = 200$. Here, $Re_\theta = \rho_e u_e \theta/\mu_e$ denotes the Reynolds number based on the boundary layer momentum thickness and M_e the Mach number at the boundary layer edge. On the present intake configuration, side walls were applied in order to avoid gradients in cross-flow direction typically generated by the expansion of the flow past the lateral intake ramp edges. The result shown in Fig. 13 indicates that due to the side walls, a highly two-dimensional flow is produced on the intake ramp and hence at the inlet to the combustion chamber.

In Fig. 14, the pressure distribution in the combustor inflow plane (see Fig. 7) is shown. The location of the shock waves generated by the lower combustor wall leading edge and the combustor side wall are clearly visible. The flow in the core region shows only small gradients in cross-flow direction.

Due to the results obtained by the three-dimensional intake flow analysis, the flow past the intake was treated in a second step as a two-dimensional flow. The constant inflow condition for this computation was determined by averaging the

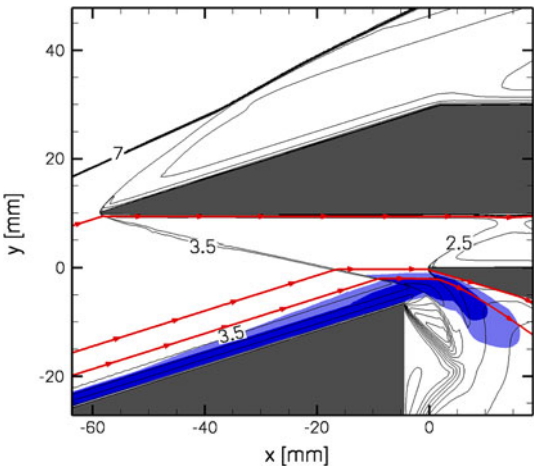

Fig. 15 Details of the computed two-dimensional intake flow field; Mach number isolines: *black* streamlines: *red* and eddy viscosity contours: *blue*

nozzle flow properties at the position of the intake. Details of the two-dimensional flow field solution in the vicinity of the combustion chamber entrance are shown in Fig. 15. The unstructured grid containing 115,000 points was adapted to the resulting shock system. Structured sub layers were used for the resolution of the boundary layers. The Mach number at the entrance of the rectangular combustion chamber duct is approximately $M = 2.5$. A significant part of the compressed flow is spilled outside the cowl and the entire intake boundary layer is swallowed by the bleed channel as indicated by the streamlines and the blue eddy viscosity contours in Fig. 15.

Static pressure profiles in the combustor inflow plane resulting from the three-dimensional and the high-resolution two-dimensional intake computation are compared in Fig. 16. Apart from the better shock resolution of the two-dimensional flow field computation, the static pressure distribution in the core region of the combustor above and below the shock wave agrees well.

Temperature, streamwise velocity and static pressure profiles in the combustor inflow plane resulting from the two-dimensional intake flow computation are shown in Fig. 17.

The computed and measured normalised surface pressure and wall heat flux on the intake ramp are compared in Figs. 18 and 19. The CFD results were obtained utilising the Wilcox k-ω and the Spalart–Allmaras turbulence models. Due to the limited spatial resolution of the heat flux measurements, the laminar to turbulent boundary layer transition process cannot be resolved in detail. However, a transition region ranging from $-220 < x < -170$ mm can be identified. As can be seen from Fig. 19, the simple $[Re_\theta/M_e]_{\text{crit}} = 200$ transition criterion, used for the computations, provides a satisfactory prediction of the transition location. Further, the plot of Fig. 19 indicates that the heat flux level downstream of

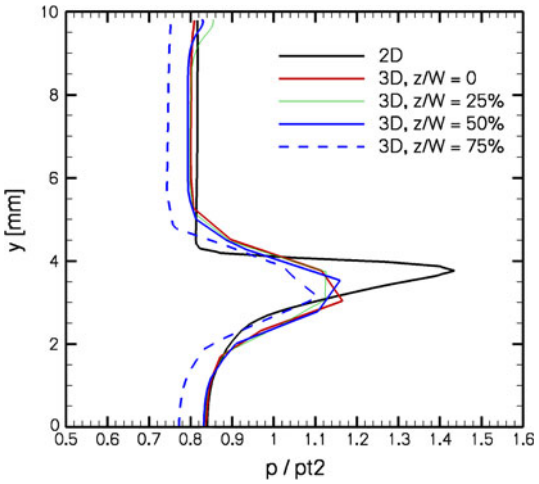

Fig. 16 Normalised static pressure profiles in the combustor inflow plane at different spanwise locations resulting from a three-dimensional intake computation compared with the result of a high-resolution two-dimensional computation (z spanwise coordinate, W half spanwidth)

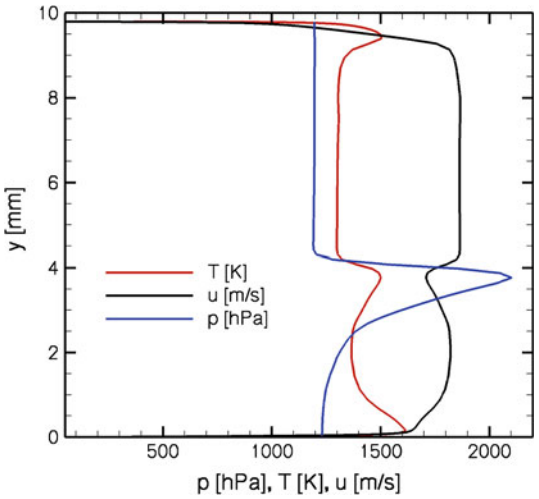

Fig. 17 Temperature, streamwise velocity and static pressure profiles in the combustor inflow plane resulting from a two-dimensional intake flow computation

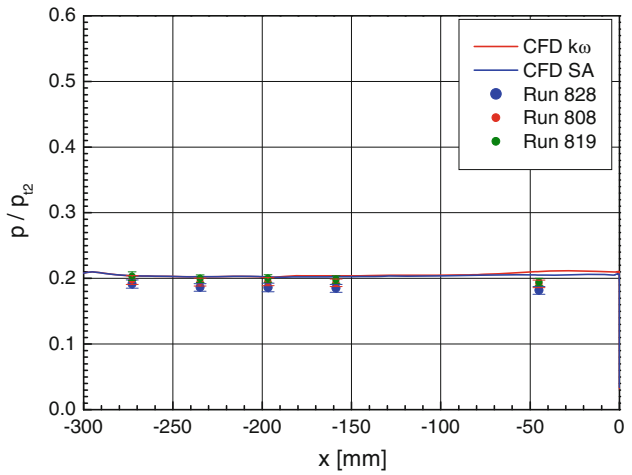

Fig. 18 Normalised surface pressure on the intake ramp; the CFD predictions result from the DLR TAU code using the Wilcox k-ω and the Spalart–Allmaras turbulence models

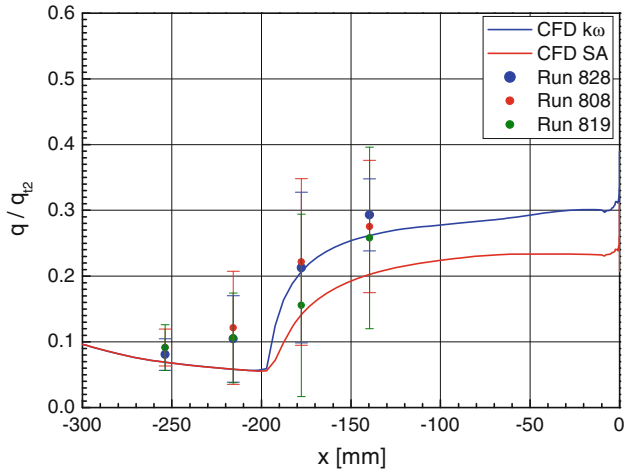

Fig. 19 Normalised wall heat flux on the intake ramp; the CFD predictions result from the DLR TAU code using the Wilcox k-ω and the Spalart–Allmaras turbulence models

the transition region is quantitatively better predicted by the computation using the Wilcox k-ω turbulence model.

It should be noted that the increase in wall heat flux due to boundary layer transition is accompanied by an increased standard deviation. This reveals the unsteady character of the flow in the transition region.

3.3 Analysis of the combustor and nozzle flow

In a first step, a three-dimensional (2,500,000 grid points) and a two-dimensional computation (440,000 grid points) of the HyShot II fuel off combustor flow were performed. The three-dimensional computational domain covered half of the combustor duct width applying a symmetry boundary condition along the centre line. The inflow conditions were derived from the three-dimensional intake computation presented in Sect. 3.2. The computed and measured normalised surface pressure distributions obtained on the lower combustor wall are compared in Fig. 20.

The profiles resulting from the computations and from the measurements agree very well. The experimental data shown here represent mean values obtained from multiple runs. In addition to the computed surface pressure data obtained on the centreline, streamwise pressure profiles along lines of 25%, 50% and 75% combustor half width are plotted in Fig. 20 revealing only slight variations in cross flow direction. Consequently, the influence of the combustor side walls on the flow properties in the vicinity of the symmetry plane can be regarded as small.

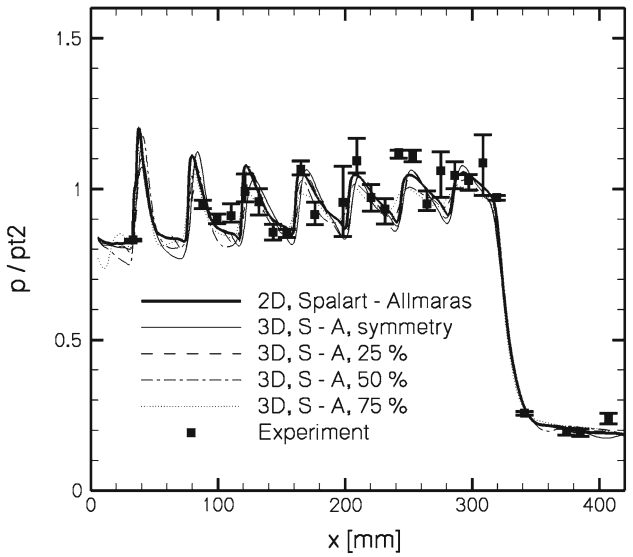

Fig. 20 Normalised computed and measured surface pressure distributions on the lower HyShot II combustor wall; fuel off condition

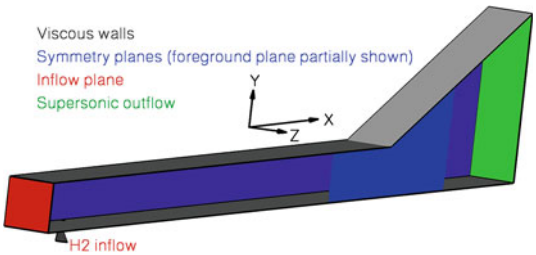

Fig. 21 Computational domain and boundary conditions used for the three-dimensional combustor fuel on computations

Based on the results obtained for the fuel-off combustor and the intake investigations, the three-dimensional computational domain shown in Fig. 21 was selected for the final set of fuel-on combustor computations.

In order to minimise the computational cost all existing flow symmetries were exploited. The combustor inflow conditions result from the two-dimensional intake computation presented in Sect. 3.2. At the outflow plane the major part of the flow is supersonic and consequently the conservative variables are extrapolated. Symmetry boundary conditions are used at the spanwise boundary planes. One is located at $z = 0$ mm cutting through the center of a porthole injector. The second symmetry plane is located at $z = 9.375$ mm representing half the distance between two injectors. Therefore, only one-eighth of the original span width of the HyShot II configuration needs to be modelled. At the bottom and top wall, viscous no-slip boundary conditions are applied. Transition from laminar to turbulent boundary layer flow at the top and bottom combustor walls is modelled using the same criterion as discussed in Sect. 3.2.

The sonic hydrogen injection was modelled by partially including the injector in the computational domain. A reservoir inflow condition as used for the HEG nozzle computations was applied at the hydrogen inflow boundary. A total hydrogen pressure of 4.6 bar and a total temperature of 300 K were prescribed resulting in a fuel equivalence ratio of $\phi = 0.295$. The fuel equivalence ratio ϕ is defined as the ratio of the fuel-to-oxidizer ratio to the stoichiometric fuel-to-oxidizer ratio: $\phi = 8\, \dot{m}_{H_2}/\dot{m}_{O_2}$.

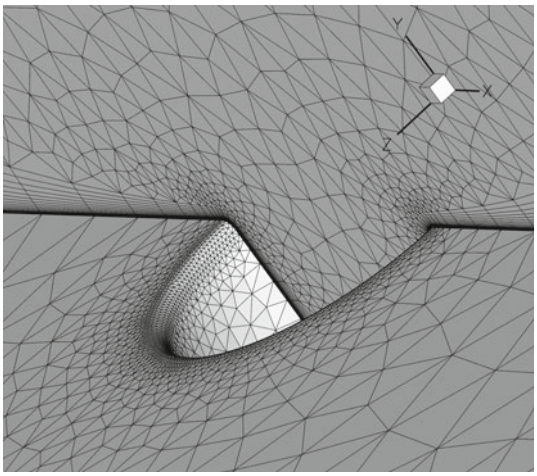

Fig. 22 Detailed view of the computational grid in the vicinity of the hydrogen injector

The grid used for the computations, discussed in the present article, consisted of about 850,000 grid points. Structured prismatic sub layers were used at the viscous walls. A dimensionless wall spacing of $y+ = O(1)$ was used to ensure sufficient resolution for the low Reynolds number turbulence models and for the computation of the wall heat flux. Outside the boundary layers, the grid points were distributed homogeneously. A detailed view of the computational grid showing the lower combustor wall and one of the spanwise symmetry planes in the vicinity of the porthole injector is given in Fig. 22.

The normalised wall pressure and heat flux distributions generated by hydrogen combustion in the HyShot II combustor on the lower and the upper walls are plotted in Figs. 23 and 24, respectively. The fuel equivalence ratio was chosen such that a steady state combustor flow was obtained. According to the design of the HyShot II flight experiment [3], the combustor is expected to show a steady-state supersonic combustion flow up to an equivalence ratio of $\phi \approx 0.35$. For clarity, the experimental data are subdivided into three groups with different ranges of fuel equivalence ratio: $0.266 < \phi < 0.288$, $0.315 < \phi < 0.329$ and $0.341 < \phi < 0.351$. The computed normalised pressure and heat flux distributions were obtained with the DLR TAU code using the Spalart–Allmaras and the Wilcox k-ω turbulence model and an equivalence ratio of $\phi = 0.295$. For all equivalence ratios, the measured wall pressure distributions are characterized by a continuous increase along the combustor indicating

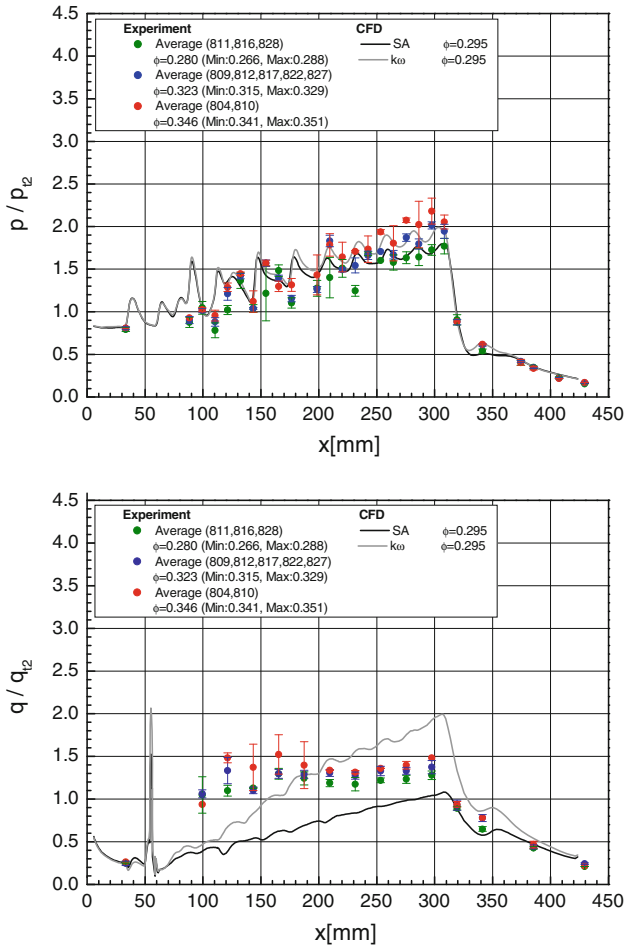

Fig. 23 Normalised computed and measured surface pressure (*top*) and wall heat flux (*bottom*) distributions on the lower HyShot II combustor wall; fuel on conditions; the *numbers in parenthesis* denote the HEG run numbers

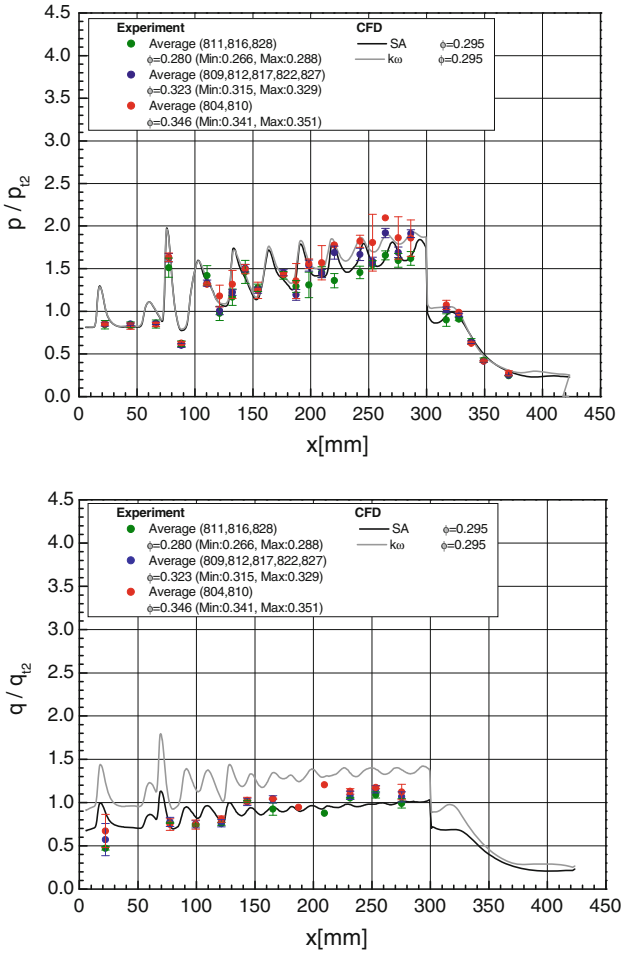

Fig. 24 Normalised computed and measured surface pressure (*top*) and wall heat flux (*bottom*) distributions on the upper HyShot II combustor wall; fuel on conditions; the *numbers in parenthesis* denote the HEG run numbers

supersonic combustion. Good agreement between the measured and the computed pressure distributions is achieved. Further, the computed normalised pressure distributions depend only weakly on the applied turbulence model.

Regarding the comparison of measured and computed wall heat flux distributions, good agreement was obtained on the upper combustor wall using the Spalart–Allmaras turbulence model (Fig. 24). However, on the lower combustor wall significant differences occur between experimental and numerical results. While the computed heat flux increases continuously downstream of the fuel injection location, the measured values remain approximately constant after an initial stepwise increase (Fig. 23). A possible reason for this discrepancy between measured and computed heat flux values could be the strong spanwise heat flux gradients obtained downstream of the hydrogen injectors. The heat flux gauges are positioned downstream of a fuel injector, and even a small flow misalignment could cause the observed discrepancy.

Grid convergence studies were performed using a coarser grid consisting of 450,000 points and a finer grid utilising 1,400,000 points. In summary, these studies showed that the differences regarding the computed surface pressure and wall heat flux distributions obtained by using the medium and the fine grid are smaller than the differences shown in Figs. 23 and 24 which resulted from using different turbulence models.

In general, the comparison of measured and computed pressure and heat flux distributions shows that the pressure generated by supersonic combustion can be predicted numerically with satisfactory accuracy. However, apart from the qualitative difference between the measured and computed heat flux distributions on the lower combustor wall, the CFD data depend strongly on the applied turbulence model. The computed peak values on the lower combustor wall differ by a factor of almost two and on the upper wall the heat flux levels differ by approximately 30%.

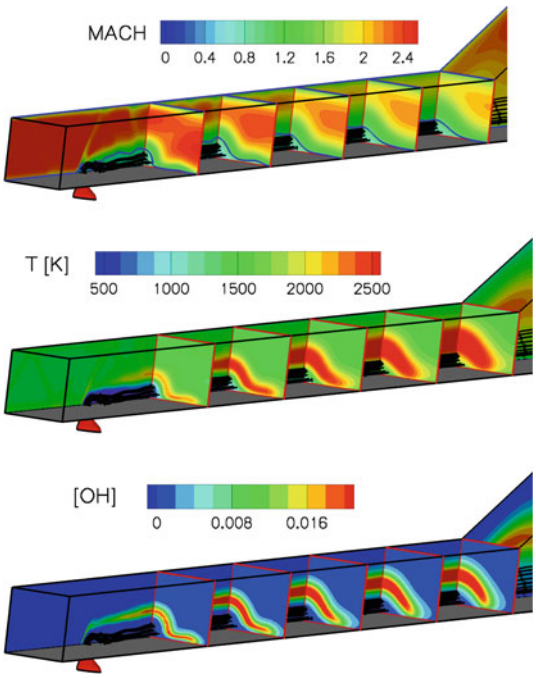

Fig. 25 Contours of computed Mach number (*top*), temperature (*middle*) and OH mass fraction (*lower*); the *black lines* represent streamlines emanating from the hydrogen injector and the *blue contour line* in the Mach number plot indicates the *sonic line*

The analysis of the computed fuel on flow field (see Fig. 25) reveals that a stable diffusion flame develops in the supersonic flow region of the HyShot II combustor. The port hole injector serves as flame anchor and the vortex system generated by the fuel injection enhances the distribution of the hydrogen in the boundary layer in cross flow direction. The gaseous hydrogen penetrates approximately one-third of the combustor height and the subsonic region downstream of the hydrogen injection covers about 10% of the cross-section area. The maximum flame temperature amounts to 2,800 K, and about 4% unburned hydrogen exists at the combustor exit.

4 Summary and conclusions

In the present article the methodology of a combined ground-based testing and numerical modelling analysis of supersonic combustion flow paths is discussed. This approach was established during the EU co-funded LAPCAT I project. The key tools are the DLR High Enthalpy Shock Tunnel Göttingen (HEG) for the ground-based free jet testing of complete scramjet configurations and the DLR TAU code for the numerical modelling of scramjet flow paths. The complete methodology can be regarded as an iterative process using both tools. This includes the determination of the wind tunnel free-stream properties and the subsequent investigation of the scramjet flow path. In order to realise an optimised CFD approach, the intake and the combustor including the exhaust surfaces are treated independently. For each component the justification of simplifying assumptions—such as symmetries or two-dimensional instead of three-dimensional flow computations—are first investigated before detailed parameter variations can be conducted (e.g. [29]).

The calibration procedure of the HEG free stream, presented here, shows the importance of measuring static pressure profiles in high-enthalpy flows. Due to the high sensitivity of this quantity to the chemical and thermal relaxation processes in the nozzle expansion, it helps to select the most suitable numerical model to determine the free-stream conditions. For the present investigations it was found that the flow in the test section is in thermal equilibrium. If measured free-stream static pressures would not be available to validate the numerical model, an error of approximately 14% would be introduced regarding the determination of the free-stream pressure if the thermal non-equilibrium model would be applied for HEG operating condition XIII. The knowledge of the absolute values of free-stream pressure and temperature is of particular importance since these quantities determine via the intake flow the combustor inflow condition, which in turn has a strong influence on the combustion process.

The comparison between computed and measured combustor surface pressure revealed that this quantity can be well predicted by the applied combustion and turbulence models. However, the numerical wall heat flux predictions are less accurate. In particular, downstream of the fuel injection location, the heat flux distributions predicted by the two different RANS turbulence models show pronounced differences when compared with each other and with the measurements. On one hand, this result calls for wall heat flux measurements with additional resolution in cross-flow direction in order to resolve the expected large heat flux gradients in this direction. Further, additional research is required regarding the modelling of turbulence. The application of DES or LES is seen as a logical next step in this context.

Acknowledgments The present work was performed within the "Long-Term Advanced Propulsion Concepts and Technologies" project investigating high-speed airbreathing propulsion. LAPCAT, coordinated by ESA-ESTEC, was supported by the EU within the 6th Framework Programme Priority 1.4, Aeronautic and Space, Contract no.: AST4-CT-2005-012282. Further info on LAPCAT can be found on http://www.esa.int/techresources/lapcat.

References

1. Steelant, J.: Achievements obtained for sustained hypersonic flight within the LAPCAT project. AIAA 2008-2578, 15th AIAA International Space Planes and Hypersonic Systems and Technologies Conference, Dayton, Ohio, USA (2008)

2. Murray, N., Steelant, J.: Methodologies involved in the Design of LAPCAT-MR1: a Hypersonic Cruise Passenger Vehicle. AIAA 2009-7399, 16th AIAA/DLR/DGLR International Space Planes and Hypersonic Systems and Technologies Conference, Bremen, Germany (2009)
3. Paull, A., Alesi, H., Anderson, S.: The HyShot flight program and how it was developed. AIAA 2002-5248, AIAA/AAAF 11th International Space Planes and Hypersonic Systems and Technologies Conference, Orleans, France (2002)
4. Smart, M.K., Hass, N.E., Paull, A.: Flight data analysis of the HyShot 2 scramjet flight experiment. AIAA J. **44**(10), 2366–2375 (2006)
5. Sunami, T., Ito, K., Sato, K., Komuro, T.: Mach 8 Ground Tests of the Hypermixer Scramjet for HyShot-IV flight Experiment. AIAA-2006-8062, AIAA/AHI 14th International Space Planes and Hypersonics Systems and Technologies Conference, Canberra, Australia, 6–9 November 2006
6. Peebles, C.: Road to Mach 10: Lessons Learned from the X-43A Flight Research Program, Library of Flight Series. AIAA (2008)
7. Hannemann, K., Schnieder, M., Reimann, B., Martinez Schramm, J.: The influence and delay of driver gas contamination in HEG. AIAA 2000-2593, 21st AIAA Aerodynamic Measurement Technology and Ground Testing Conference, Denver, CO, 19–22 June 2000
8. Hannemann, K.: High Enthalpy Flows in the HEG Shock Tunnel: Experiment and Numerical Rebuilding. 41st AIAA Aerospace Sciences Meeting and Exhibit, 6–9 Jan, Reno, Nevada (2003)
9. Hannemann, K., Martinez Schramm, J., Karl, S.: Recent extensions to the High Enthalpy Shock Tunnel Göttingen (HEG). In: Proceedings of the 2nd International ARA Days "Ten Years after ARD", Arcachon, France, 21–23 October 2008
10. Saito, T., Ono, F., Kobayashi, K., Kudo, K., Takegoshi, M., Ueda, S.: Firing Tests of a Liquid-Hydrogen-Cooling Scramjet Engine in the Ramjet Engine Test Facility II. AIAA 2005-3821, 41st AIAA/ASME/SAE/ASEE Joint Propulsion Conference & Exhibit, Tucson, Arizona (2005)
11. Garrard, D., Rigney, S., Bates, B.: Progress Report on the APTU Upgrade Activities. AIAA 2004-2496, 24th AIAA Aerodynamic Measurement Technology and Ground Testing Conference, Portland, Oregon (2004)
12. Gerhold, T., Friedrich, O., Evans, J., Galle, M.: Calculation of Complex Three-Dimensional Configurations Employing the DLR-TAU-Code. AIAA 1997-0167 (1997)
13. Reimann, B., Johnston, I., Hannemann, V.: The DLR TAU-Code for High Enthalpy Flows. Notes on Numerical Fluid Mechanics and Multidisciplinary Design, vol. 87. Springer, Berlin (2004)
14. Spalart, P.R., Allmaras, S.R.: A One-Equation Turbulence Model for Aerodynamic Flows. AIAA 1992-0439 (1992)
15. Wilcox, D.C.: Turbulence Modelling for CFD. DCW Industries, La Canada, California (1998)
16. Liou, M.S., Edwards, J.R.: AUSM Schemes and Extensions for Low Mach and Multiphase Flows. 30th Computational Fluid Dynamics Lecture Series, Von Karman Institute for Fluid Dynamics (1999)
17. Gerlinger, P.: An implicit multigrid method for turbulent combustion. J. Comput. Phys. **167**, 247–276 (2001)
18. Wilke, C.R.: A viscosity equation for gas mixtures. J. Chem. Phys. **18**(4) (1950)
19. Herning, F., Zipperer, L.: Beitrag zur Berechnung der Zähigkeit technischer Gasgemische aus den Zähigkeitswerten der Einzelbestandteile. Das Gas- und Wasserfach, vol. 79, pp. 49–54, 69–73 (1936)
20. Landau, L.D., Teller, E.: Zur Theorie der Schalldispersion (on the theory of sound dispersion). Phys. Z. Sowjetunion **10**(34), 34–43 (1936)
21. Millikan R.C., White D.R.: Systematics of vibrational relaxation. J. Chem. Phys. **39**(12), 3209–3213 (1963)
22. Gaffney, R.L., White, J.A., Girimaji, S.S., Drummond, J.P.: Modeling Turbulent Chemistry Interactions using Assumed PDF Methods. 28th AIAA/SAE/ASME/ASEE Joint Propulsion Conference and Exhibit (1992)
23. McIntosh, M.K.: Computer Program for the Calculation of Frozen and Equilibrium Conditions in Shock Tunnels. Australian National University, Canberra (1968)
24. Gupta, R.N., Yos, J.M., Thompson, R.A., Lee, K.P.: A Review of Reaction Rates and Thermodynamic and Transport Properties for an 11-Species Air Model for Chemical and Thermal Nonequilibrium Calculations to 30000 K. NASA Reference Publication, No. 1232 (1990)
25. Hannemann, K., Martinez Schramm, J.: High enthalpy, high pressure short duration testing of hypersonic flows. In: Tropea, C., Foss, J., Yarin, A. (eds.) Springer Handbook of Experimental Fluid Mechanics, pp. 1081–1125. Springer, Berlin (2007)
26. Owen, R. Cain, T.: Reconstruction of the Hyshot-2 Flight from onboard sensors. In: Proceedings of the Fifth European Symposium on Aerothermodynamics for Space Vehicles, Cologne, Germany, 8–11 November 2004
27. Karl, S., Hannemann, K., Mack, A., Steelant, J.: CFD Analysis of the HyShot II Scramjet Experiments in the HEG Shock Tunnel. AIAA 2008-2548, 15th AIAA International Space Planes and Hypersonic Systems and Technologies Conference, Dayton, Ohio (2008)
28. Bertin, J.J., Stetson, K.F., Bouslog, S.A., Caram, J.M.: Effect of isolated roughness elements on boundary-layer transition for shuttle orbiter. J. Spacecr. Rockets **34**(4), 426–436 (1997)
29. Mack, A., Steelant, J., Martinez-Schramm, J., Hannemann, K.: Sensitivity Analysis for the HyShot Generic Supersonic Combustion Configuration using CFD, ISABE-2007-1310. 18th International Symposium on Airbreathing Engines, Beijing (2007)